INSTITUTE OF PHYSICS PUBLISHING NETWORK: COMPUTATION IN NEURAL SYSTEMS

Network: Comput. Neural Syst. **13** (2002) 41–66 PII: S0954-898X(02)29889-9

Information transfer in entrained cortical neurons

P H E Tiesinga[1], J-M Fellous[1], J V José[1,2] and T J Sejnowski[1,3]

[1] Sloan-Swartz Center for Theoretical Neurobiology, Computational Neurobiology Laboratory and Howard Hughes Medical Institute, Salk Institute, La Jolla, CA 92037, USA
[2] Center for Interdisciplinary Research on Complex Systems, Department of Physics, Northeastern University, Boston, MA 02115, USA
[3] Department of Biology, University of California San Diego, La Jolla, CA 92093, USA

E-mail: tiesinga@salk.edu

Received 30 December 2000
Published 14 November 2001
Online at stacks.iop.org/Network/13/41

Abstract

Cortical interneurons connected by gap junctions can provide a synchronized inhibitory drive that can entrain pyramidal cells. This was studied in a single-compartment Hodgkin–Huxley-type model neuron that was entrained by periodic inhibitory inputs with low jitter in the input spike times (i.e. high precision), and a variable but large number of presynaptic spikes on each cycle. During entrainment the Shannon entropy of the output spike times was reduced sharply compared with its value outside entrainment. Surprisingly, however, the information transfer as measured by the mutual information between the number of inhibitory inputs in a cycle and the phase lag of the subsequent output spike was significantly increased during entrainment. This increase was due to the reduced contribution of the internal correlations to the output variability. These theoretical predictions were supported by experimental recordings from the rat neocortex and hippocampus *in vitro*.

1. Introduction

The spike trains from neurons recorded from the cerebral cortex *in vivo* are highly variable (see Shadlen and Newsome 1998). Similar spike trains can be studied *in vitro* by injecting a fluctuating current at the soma or by stimulating afferent synaptic inputs (Stevens and Zador 1998, Harsch and Robinson 2000, Salinas and Sejnowski 2000). Despite high variability, neurons can fire with high temporal precision and reliability (Berry *et al* 1997, Warland *et al* 1997, Reich *et al* 1997, Berry and Meister 1998, Buracas *et al* 1998, Bair 1999). Precision is defined as the inverse of the temporal jitter in the spike times and reliability is a measure for the reproducibility of spikes across trials. Precision and reliability are highest *in vitro* when neurons are driven by an input containing high-frequency components (Mainen and Sejnowski 1995, Nowak *et al* 1997, Tang *et al* 1997, Warzecha *et al* 1998, Cecchi *et al* 2000) or in response to a sinusoidal input current at 'resonant' frequencies (Hunter *et al* 1998, Fellous *et al* 2001).

0954-898X/02/010041+26$30.00

Recent information-theoretical analyses of the neuronal spike trains in the fly (de Ruyter van Steveninck *et al* 1997, Warzecha and Egelhaaf 1999) and in the cat lateral geniculate nucleus (Reinagel *et al* 1999, Reinagel and Reid 2000) indicate that the precise spike times contain more information about the input than the firing rate alone. The question of how the information encoded by these precise spike times could be used in cortex is an open problem (Shadlen and Newsome 1994, Softky 1995, Gur and Snodderly 1997, Shadlen and Newsome 1998, Oram *et al* 1999, Wiener and Richmond 1999).

A number of studies have examined how a periodic excitatory synaptic drive affects the spikes of integrate-and-fire (IAF) model neurons (Gerstner *et al* 1996, Kempter *et al* 1998, Burkitt and Clark 1999, 2000). The precision of IAF neurons driven by excitatory postsynaptic potentials decreases with increasing input jitter and increases with the number of correlated inputs (Burkitt and Clark 2000). In modelling studies (Lytton and Sejnowski 1991, Kistler and van Hemmen 1999, Tiesinga and José 2000, Tiesinga and Sejnowski 2001) and a number of experiments (Cobb *et al* 1995, Koos and Tepper 1999, Jaeger and Bower 1999, Gauck and Jaeger 2000, Tamas *et al* 2000) inhibitory inputs were highly effective in controlling the precise spike times of postsynaptic neurons. For example, the reliability and precision of cerebellar neurons increased with the amount of correlation (or synchronization) and precision of the inhibitory inputs (Gauck and Jaeger 2000).

Local cortical interneurons of the same type are connected by gap junctions (Galarreta and Hestrin 1999, Gibson *et al* 1999, Beierlein *et al* 2000). As a result local interneuron networks readily synchronize (Deans *et al* 2001, Hormuzdi *et al* 2001) and project synchronous inhibition to principal cells and other interneurons. The putative function of synchronized inhibition is an open question (Galarreta and Hestrin 2001a, 2001b, José *et al* 2001).

We investigate here how a varying inhibitory synaptic drive affects the information transduction by a neuron. A biophysical model neuron with Hodgkin–Huxley-type currents is used to study how information could be transmitted by the spiking activity of a synchronized network of interneurons. Entrainment reduces the information capacity of the spike times, but as we show here, it enhances the transmitted information as measured by the mutual information between the input and the output spike times. The results of this theoretical analysis are supported by recordings from neocortical and hippocampal neurons studied *in vitro*. Some of these results were reported earlier in abstract form (Tiesinga *et al* 2001b).

2. Methods

2.1. Biophysical model

The model system consisted of a synchronized network of interneurons projecting via fast GABAergic synapses to a single postsynaptic neuron (figure 1(*a*)). The postsynaptic neuron could be either another interneuron or a regular or fast spiking neocortical pyramidal neuron. The postsynaptic neuron was sufficiently depolarized to spike periodically in the absence of synaptic inputs. The presynaptic network produced a periodic population discharge with temporal jitter σ_{in}, although individual presynaptic neurons need not fire on each cycle (figure 1(*b*)). The firing rate histogram (FRH) of the simulated interneuron network input consisted of a periodic sequence (period $T = 25$ ms) of Gaussian probability density functions with variance σ_{in}^2, mean $(m + \frac{1}{2})T$, with $m = 0, 1, \ldots$, and presynaptic firing rate f_{pre} equal to the FRH (bin width $\mathrm{d}t = 0.01$ ms) summed over one second. A spike was generated when a random number drawn from a uniform distribution between zero and unity at each time step was smaller than or equal to the value of the FRH. In principle, a random number should be generated each time step for each presynaptic neuron. Here we generated only five random numbers each time step. This was a good approximation for the f_{pre} values used here.

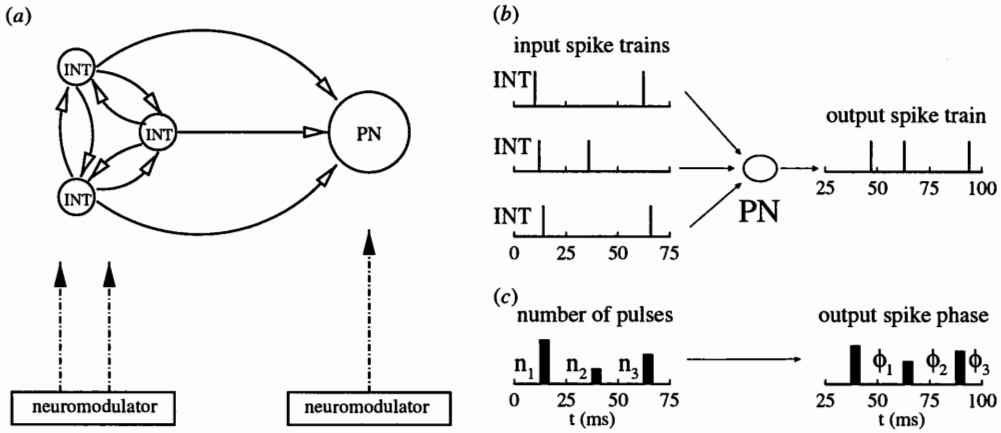

Figure 1. Information encoding in neuronal spike trains. (*a*) Postsynaptic neuron (PN) receives inputs from a synchronized network of inhibitory neurons (INT). A depolarizing drive to the neurons simulates the effects of neuromodulators. (*b*) Individual presynaptic neurons (INT) fire at a fixed average phase with temporal jitter σ_{in} and sometimes skip cycles. The postsynaptic neuron produces a spike on each cycle when it is 1:1 entrained. (*c*) The number n_i of active neurons in cycle i is mapped onto the output spike phase ϕ_i in the next cycle. The mutual information between the phases and the number of active input neurons is a measure of the information encoded in the spike timing.

Samples of spike trains are shown in figure 1(*b*). The number n_i of presynaptic pulses in cycle i was variable and represented the signal to be transmitted. Its average value was $n_{\text{pre}} = f_{\text{pre}}/(40\text{ Hz})$ and when FRH $\ll 1$ the variance, σ_n^2, was also equal to n_{pre}. Each spike produced an exponentially decaying conductance pulse in the postsynaptic cell, yielding a current $I_{\text{syn}} = g_i \exp(-t/t_i)(V - E_{\text{GABA}})$. In this expression t is the time since the presynaptic pulse arrival, $t_i = 10$ ms is a decay constant, g_i the unitary synaptic conductance, V the postsynaptic membrane potential and $E_{\text{GABA}} = -75$ mV is the reversal potential. In the simulations $f_{\text{pre}} g_i = 5\text{ mS cm}^{-2}\text{ Hz}$ and f_{pre} was varied between 2.5 and 20 kHz ($n_{\text{pre}} = 62.5$–500), corresponding to the activity of 100–1000 presynaptic neurons. The maximum total conductance per cycle was between 0.1 and 0.5 mS cm^{-2}, similar to values used previously (Wang and Buzsáki 1996).

The resulting train of conductance pulses drove a single-compartment neuron with Hodgkin–Huxley-type voltage-gated sodium and potassium channels, a passive leak current, the synaptic currents described above; an intrinsic noise source with variance $2D$ and an applied current I_0 representing the membrane depolarization caused by neuromodulators, such as, for instance, acetylcholine (figure 1(*a*)). The intrinsic noise includes internal variability from channel noise and other synaptic inputs uncorrelated with the inhibitory drive. A detailed description of the model neuron is in the appendix and its implementation in the Fortran programming language was given in Tiesinga and José (2000). This formulation accurately represents the spike generation in fast and regular spiking cortical pyramidal cells (McCormick *et al* 1985) and hippocampal interneurons (Wang and Buzsáki 1996). In the following g_{max} and g_i have units mS cm^{-2}; I_0 is in μA cm^{-2}; f_{pre} is in Hz; ϕ_i, σ_{out}, σ_{in} and T are in ms; n_i, n_{pre} and σ_n are dimensionless.

2.2. *Experimental details*

Protocols for these experiments were approved by the Salk Institute Animal Care and Use Committee and they conform to USDA regulations and NIH guidelines for humane care and

use of laboratory animals. Coronal slices of rat pre-limbic and infra-limbic areas of prefrontal cortex as well as transversal slices of hippocampus, were obtained from 2 to 4 weeks old Sprague-Dawley rats. Rats were anaesthetized with metofane (Methoxyflurane, Mallinckrodt), and decapitated. Their brains were removed and cut into 350 μm thick slices on a Vibratome 1000. Slices were then placed in a submerged chamber containing artificial cerebrospinal fluid (ACSF, mM: NaCl, 125; NaH_2CO_3, 25; D-glucose, 10; KCl, 2.5; $CaCl_2$, 2; $MgCl_2$, 1.3; NaH_2PO_4, 1.25) saturated with 95% O_2/5% CO_2, at room temperature. Whole-cell patch-clamp recordings were achieved using glass electrodes containing 4–10 MΩ, mM: $KMeSO_4$, 140; Hepes, 10; NaCl, 4; EGTA, 0.1; Mg-ATP, 4; Mg-GTP, 0.3; phosphocreatine, 14. Patch-clamp was performed under visual control at 30–32 °C. In most experiments Lucifer Yellow (RBI, 0.4%) or Biocytin (Sigma, 0.5%) was added to the internal solution in order to visualize neurons after the recording session. In all experiments, NMDA synapses were blocked by D-2-amino-5-phosphonovaleric acid (D-APV, 50 μM), AMPA synapses were blocked by 6,7-dinitroquinoxaline-2,3-dione (DNQX, 10 μM), and $GABA_A$ synapses were blocked by Biccuculine methiodide (Bicc, 20 μM). Bicc also partially blocked calcium-dependent potassium channels. All drugs were obtained from RBI or Sigma, freshly prepared in ACSF and bath applied. Data were acquired with Labview 5.0 and a PCI-16-E1 data acquisition board (National Instrument), and analysed with MATLAB (The Mathworks) and Excel (Microsoft). We used regularly spiking layer 5 pyramidal cells. Interneurons were recorded from cortical layer 5/6 and stratum radiatum of hippocampus and were characterized by high firing rates, no adaptation and prominent fast spike re-polarization. Both pyramidal cells and interneurons were identified morphologically.

Current was injected into the neuron to mimic the effect of a synaptic drive. Each trial lasted between 2000 and 4000 ms. The presynaptic spike train was generated as in the model simulations. Each presynaptic spike generated an exponentially decaying hyperpolarizing current pulse with amplitude A/n_{pre} that simulated the effect of an inhibitory postsynaptic potential. We varied A between 0.1 and 0.2 nA and n_{pre} between 5 and 200. A depolarizing constant current was added to make the neuron spike in the presence of the hyperpolarizing pulses. The average injected current, a, was constant (a typical value was between 0.05 and and 0.12 nA) for the different values of n_{pre} used during the recording session. The injected current was calculated off line and supplied to Labview as a computer file with a sampling rate of 10 kHz. A gain factor G was adjusted on line to make the neuron spike once on each cycle, that is 1:1 entrainment. In some cases 1:1 entrainment could not be reached with the neuron still generating action potentials that exceeded 20 mV. The gain G was between 1 and 4.5.

2.3. *Information-theoretical analysis*

The neuron maps a particular value of n_i into a spike phase ϕ_i (figure 1(*c*)). The spike phase ϕ is the spike time modulo T. We calculated the entropy S_n of the input distribution P_n (the bin width was 1) and the entropy S_ϕ of the phase histogram P_ϕ (with a bin width of 1 ms),

$$S_n = \sum_i P_n(i) \log_2 P_n(i), \tag{1}$$

$$S_\phi = \sum_j P_\phi(\hat{\phi}_j) \log_2 P_\phi(\hat{\phi}_j), \tag{2}$$

where $\hat{\phi}_j = j + \frac{1}{2}$ is the centre of the jth bin, and $j = 0, 1, \ldots, 24$.

The mutual information per spike was (Shannon and Weaver 1949, Cover and Thomas 1991)

$$M_{n\phi} = S_n + \sum_j \left[P_\phi(\hat{\phi}_j) \sum_n P_{n\phi}(n|\hat{\phi}_j) \log_2 P_{n\phi}(n|\hat{\phi}_j) \right],$$

and measured, on average, how much the uncertainty in the input was reduced by knowing the output (Buracas and Albright 1999, Borst and Theunissen 1999). The joint probability distribution $P_{n\phi}$ was obtained by counting the data points (ϕ_i, n_i), $i = 1, 2, \ldots$, in a two-dimensional set of bins (bin size was 1 ms by 1). The sampling error in $M_{n\phi}$ was estimated as the mutual information between n and ϕ, when drawn independently from their respective marginal distributions, P_n and P_ϕ, using the same number of data points as for $M_{n\phi}$ itself. Other authors have used a reconstruction method to estimate $M_{n\phi}$ (Rieke *et al* 1997, Wessel *et al* 1996). Their method yields a lower bound for $M_{n\phi}$, whereas the expression used here is, in principle, exact. The transmitted information for a given set of parameters, I_0, σ_{in}, f_{pre} and D, cannot exceed the minimum, S_{min}, of S_ϕ and S_n. Hence, when either S_n or S_ϕ is zero at the specified bin width, the signal is not transmitted by the neuron. This happened when the output jitter was much smaller than the bin width so that all spike phases fell in one bin. The bin width of 1 ms used here is consistent with previous results on typical spike-time precisions (Mainen and Sejnowski 1995, Reinagel and Reid 2000). The maximum of S_{min} averaged over all input distributions P_n is an upper bound of the channel capacity. The output jitter σ_{out} was defined as the standard deviation of the phase distribution and the firing rate was the inverse of the average interspike interval.

A similar information-theoretical analysis was applied to the experimental recordings. The output spike phase ϕ_i and the number n_i of input spikes were pooled together across different trials after discarding a transient. The length of the transient, between 200 and 1000 ms, was determined by visual inspection of the intracellular voltage recordings and the rastergram (defined below). In some cases the length of the transient was varied to assay the robustness of the measured statistics. The bin width for the phase distribution was between 1 and 4 ms so that the sampling error did not exceed 50% of $M_{n\phi}$. The bin width was 1 ms (as in the model simulations) whenever possible. When the number of different values of n_i observed during a run was less than ten, each different value was assigned to a different bin. Otherwise the range between the minimum and maximum value of n_i was divided into ten bins of equal size. To gain qualitative insight in the mutual information we also plotted the conditional average $\langle n \rangle$ and its standard deviation for a fixed output phase.

The firing rate was calculated as the number of spikes per trial, excluding the transient, divided by the remaining length of the trial. Each spike was plotted as a small tick in the rastergram, the x-ordinate was the spike time and the y-ordinate the trial number. The FRH was determined with a bin width equal to the cycle length. Its value was the number of trials in which a spike was obtained during that cycle. The FRH, averaged over all cycles, yielded an estimate of the spike-time reliability.

3. Results

3.1. Dynamics of a neuron driven by noisy periodic spike trains

A neuron driven by a periodic force can become entrained. Consider, for instance, a neuron driven by a sinusoidal current, $I_{\text{sin}}(t) = I_0 + I_f \cos 2\pi f_d t$, with $I_f = 1.0\ \mu\text{A cm}^{-2}$ and $f_d = 40$ Hz. The firing rate f versus current, I_0, curve was characterized by steps on which f was constant and equal to $\frac{p}{q} f_d$ for a range of I_0 values (figure 2(*a*)i). The neuron produced p spikes per q periods and the output spike train repeated itself after q cycles. In this study the neuron was driven by noisy presynaptic inhibitory spike trains. Noise is in general detrimental to phase locking. For the values of σ_{in} and f_{pre} used here, only the 1:1 and higher order integer steps ($q = 1$) remained (figure 2(*a*)ii). Here the 1:1 steps were used to explore information transduction.

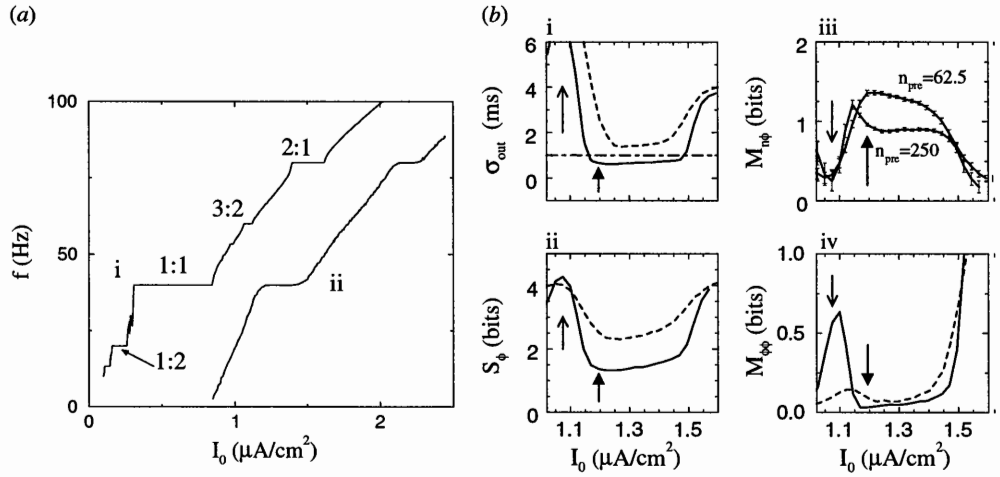

Figure 2. Entrainment of the model neuron as the amplitude I_0 of the current injection is varied. (*a*) Comparison between i, a sinusoidal current with amplitude $I_f = 1.0\ \mu\text{A cm}^{-2}$ and frequency $f_d = 40$ Hz; and ii, noisy synaptic drive with $n_{\text{pre}} = 62.5$, $\sigma_{\text{in}} = 1$ and $g_i = 0.002$. Averages are over 4000 cycles, after discarding a transient of 40 cycles. (*b*) Dynamics of a 1:1 entrained neuron driven by noisy presynaptic spike trains. i, σ_{out}; ii, S_ϕ; iii, $M_{n\phi}$, and iv, $M_{\phi\phi}$ versus current I_0. Parameters: $T = 25$, $\sigma_{\text{in}} = 1$ (indicated by the dot–dashed line in i), and (solid curves) $n_{\text{pre}} = 250$ and $g_i = 0.0005$, (dashed curves) $n_{\text{pre}} = 62.5$ and $g_i = 0.002$. Averages are over 2×10^4 cycles, after discarding a transient of 20 cycles. Arrows are discussed in the text.

3.2. Improved information transduction on the entrainment step

For the synaptic strength used here the output jitter σ_{out} was smaller than the input jitter σ_{in} only on entrainment steps. An example is shown in figure 2(*b*) for $\sigma_{\text{in}} = 1$ and $n_{\text{pre}} = 250$. At $I_0 = 1.1$, σ_{out} was still above 5 ms (solid curve in figure 2(*b*)i). Increasing the current drove the neuron into entrainment, and σ_{out} dropped to below $\sigma_{\text{in}} = 1$ ms (σ_{in} is the dot–dashed curve in figure 2(*b*)i). The output entropy, S_ϕ, is closely related to the width of the spike-phase distribution, and it dropped from 4.2 bits to less than 1.5 bits per spike (solid curve in figure 2(*b*)ii). The mutual information $M_{n\phi}$, however, went from a value close to zero, to approximately one bit per spike (figure 2(*b*)iii). The coding fraction $C_{n\phi} = M_{n\phi}/S_\phi$ went from close to zero to about 60% (data not shown). To investigate this further, the map of the output spike phase, ϕ, versus the number of inputs per cycle, n, when the neuron was entrained was compared to the map for currents off the entrainment step (figure 3).

Because a given ϕ was reached from a large range of n values off the entrainment step (figure 3(*a*)), a particular ϕ value revealed little about the input that produced it and the mutual information was low (open arrow in figure 2(*b*)iii). During entrainment the input n was mapped onto a small range of ϕ values (figure 3(*b*)) leading to higher precision (filled arrow in figure 2(*b*)i). Furthermore, the observed value of ϕ varied linearly with the input n (figure 3(*b*)). When ϕ is observed, the uncertainty about the input is reduced and the mutual information is increased (filled arrow in figure 2(*b*)iii).

The mutual information $M_{\phi\phi}$ between the phase ϕ_i in the present cycle and ϕ_{i+1} in the next cycle quantifies the reduction in the uncertainty about the next phase given the present phase. The return map, $\phi_i \rightarrow \phi_{i+1}$, is shown in figures 3(*c*) and (*d*). During entrainment the observed phases were approximately independent and the mutual information was close to zero (filled arrow in figure 2(*b*)iv). The spike phase fluctuated around a well defined average and the

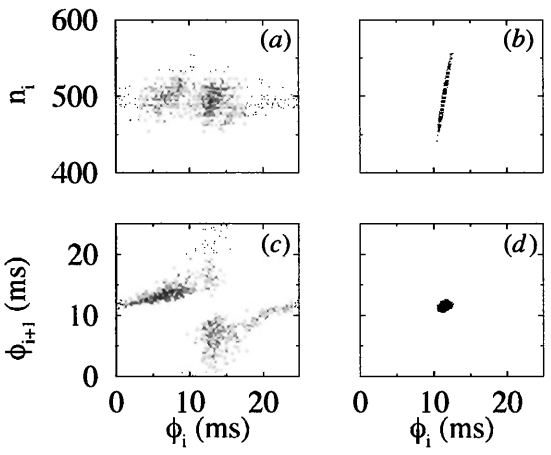

Figure 3. Comparison between neuronal spike timing in entrained (*b*), (*d*) and non-entrained (*a*), (*c*) states. The map $\phi_i \rightarrow n_i$ (*a*), (*b*), and the return map $\phi_i \rightarrow \phi_{i+1}$ (*c*), (*d*) are shown. Here (*a*), (*c*) $I_0 = 1.075$, and (*b*), (*d*) $I_0 = 1.195$. $n_{\text{pre}} = 500$, $g_i = 2.5 \times 10^{-4}$ and $\sigma_{\text{in}} = 1$.

return map was a compact cluster of points (figure 3(*d*)). In contrast, without entrainment the points in the return map were spread out over all possible values of the phase (figure 3(*c*)). A given value of ϕ_i mapped onto a distribution of ϕ_{i+1} values that was different from the total distribution (and also had a different mean). The mutual information of this distribution could be higher than one bit per spike (open arrow, figure 2(*b*)iv).

Simulations were also performed for a smaller number of presynaptic inputs, $n_{\text{pre}} = 62.5$. The unitary strength of the inhibitory conductance was increased by a factor of four so that the total injected conductance remained the same. The output jitter was again reduced during entrainment compared with outside entrainment (dashed curve in figure 2(*b*)i). However, it remained larger than the input jitter $\sigma_{\text{in}} = 1$ ms. The output entropy, S_ϕ, transmitted information, $M_{n\phi}$, and mutual information $M_{\phi\phi}$ during entrainment were increased compared with their values for $n_{\text{pre}} = 250$ (dashed and solid curves in figures 2(*b*)ii–iv, respectively). The behaviour of the transmitted information as a function of n_{pre} is studied in the next section. Note that outside entrainment $M_{\phi\phi}$ was reduced compared with its value for $n_{\text{pre}} = 250$.

3.3. Information transduction depends on σ_{in} and n_{pre}

We have varied the average number of input pulses per cycle, n_{pre}, such that the average total synaptic conductance, proportional to $n_{\text{pre}} g_i$, stayed constant: when n_{pre} was increased, g_i decreased as $1/n_{\text{pre}}$. For large values of n_{pre}, P_n had approximately a Gaussian probability distribution with variance n_{pre} and entropy S_n proportional to $\log_2 n_{\text{pre}}$ (Shannon and Weaver 1949). The relative variations σ_n/n_{pre} in the number of presynaptic pulses per cycle decreased as $1/\sqrt{n_{\text{pre}}}$ and consequently σ_{out} and S_ϕ decreased with increasing n_{pre} (figure 4(*a*)). The mutual information $M_{n\phi}$ had an optimum as a function of n_{pre} (figure 4(*b*)).

The decrease of $M_{n\phi}$ at large n_{pre} occurs because the biophysical size of the signal the—conductance change—is reduced for higher n_{pre}, while the strength of input jitter stays the same. It becomes more difficult to distinguish the signal-induced jitter from the noise-induced output jitter at the resolution set by the bin width.

Small n_{pre} values yielded large relative fluctuations $\Delta n_i/n_{\text{pre}}$ in the input ($\Delta n_i = n_i - n_{\text{pre}}$), leading to a large value of σ_{out}. The resulting nonlinear phase dynamics tended to reduce $M_{n\phi}$. For even larger positive $\Delta n_i/n_{\text{pre}}$, the neuron might not spike on the next cycle or could spike twice in the same cycle for large negative $\Delta n_i/n_{\text{pre}}$. It took a number of cycles for ϕ_i to converge back to its stationary value, leading to long-time correlations between the phases,

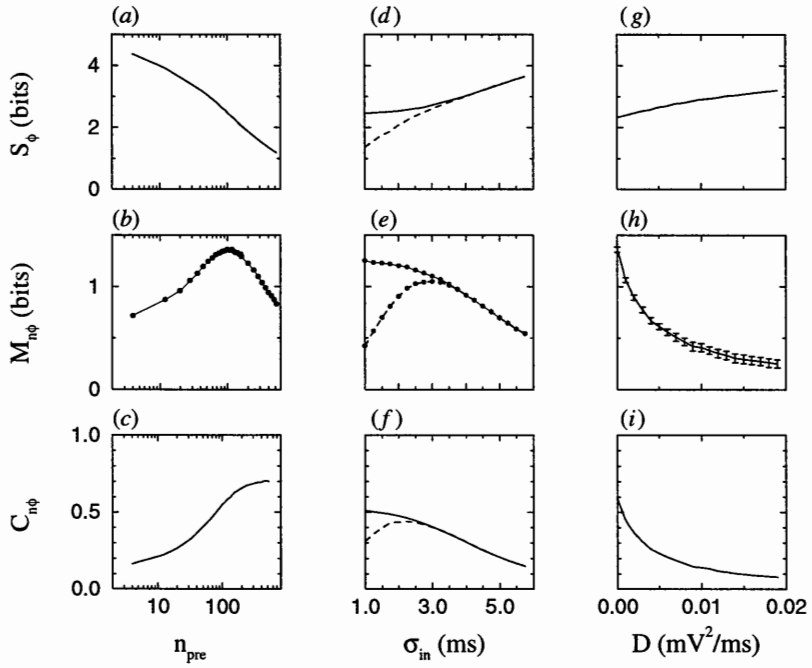

Figure 4. Dependence of information transfer of a model neuron on input spike train parameters. (*a*), (*d*), (*g*) Output entropy S_ϕ; (*b*), (*e*), (*h*) mutual information $M_{n\phi}$ and (*c*), (*f*), (*i*) coding fraction $C_{n\phi}$ as a function of (*a*)–(*c*) the number of input spikes n_{pre}; (*d*)–(*f*) input jitter σ_{in} and (*g*)–(*i*) intrinsic noise strength D. Parameters were (*a*)–(*c*) $I_0 = 1.2$, $\sigma_{in} = 1$, and $D = 0$; (*d*)–(*f*) $n_{pre} = 62.5$, $I_0 = 1.35$, and $D = 0$; (*g*)–(*i*) $n_{pre} = 62.5$, $I_0 = 1.25$, and $\sigma_{in} = 1$. In (*d*)–(*f*) dashed curves are results for synaptic saturation at $g_{max} = 0.1$; solid curves are results without synaptic saturation effects (the default). In (*b*), (*e*) the sampling errors are smaller than the symbol size; in (*h*) they are indicated by the error bars. Averages are over 40×10^3 cycles after discarding a transient of 40 cycles.

hence $M_{n\phi}$ was reduced even further. This accounts for the increase in $M_{n\phi}$ when n_{pre} is increased for small values of n_{pre} (figure 4(*b*)).

As the input spike-time jitter, σ_{in}, was increased, the transduced information, $M_{n\phi}$ and $C_{n\phi}$, was reduced, even though S_ϕ increased (solid curves in figures 4(*d*)–(*f*)). For large values of σ_{in} the neuron missed spikes during some cycles, or spiked twice on other cycles, further reducing $M_{n\phi}$, as discussed before. When intrinsic noise—noise unrelated to the synaptic input—was added to the neuron, $M_{n\phi}$ and $C_{n\phi}$ decreased, while S_ϕ increased, with increasing noise strength D (figures 4(*g*)–(*i*)).

Limited synaptic resources might affect information transduction. We have modelled the effect of whole-cell synaptic saturation by imposing a maximum synaptic conductance g_{max}. Additional presynaptic spikes were ignored when the synaptic conductance exceeded g_{max}. For $g_{max} = 0.1$ this happened when more than 50 spikes arrived simultaneously. Hence, for $n_{pre} = 62.5$, the mutual information was reduced for small presynaptic input jitter (dashed curve in figure 4(*e*)). This led to an optimum value for $M_{n\phi}$ at $\sigma_{in} = 3$ and for $C_{n\phi}$ at $\sigma_{in} = 2.25$ (dashed curves in figures 4(*e*) and (*f*)). Noise in the form of presynaptic input jitter can therefore improve signal transduction.

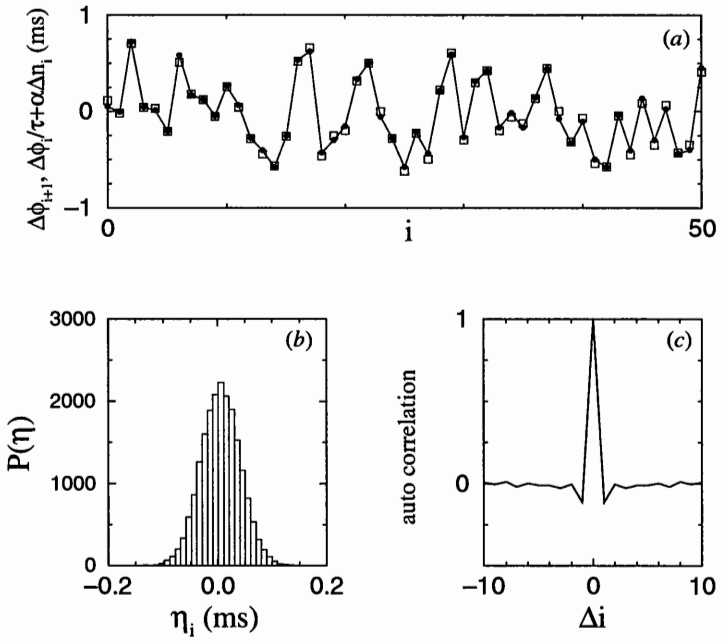

Figure 5. Linear map predicts the phase dynamics of a 1:1 entrained model neuron. (*a*) Observed phase deviation $\Delta\phi_{i+1}$ (solid circles) and predicted value, $\Delta\phi_i/\tau + \alpha\Delta n_i$ (open squares), as a function of cycle index i. (*b*) Histogram of the difference η_i between observed and predicted value. (*c*) The autocorrelation of η_i as a function of time-lag Δi. Model data as in figure 3(*b*), $\alpha = 0.0177$, $\tau = 3.70$, $\sigma_n = 19$ and $\sigma_\eta = 0.036$.

3.4. Information transmission in the linear-map approximation

The dynamics of the phase on the entrainment step (see figure 3(*b*)) could be approximated by a linear map:

$$\Delta\phi_{i+1} = \frac{1}{\tau}\Delta\phi_i + \alpha\Delta n_i + \eta_i. \tag{3}$$

Here $\Delta\phi_i = \phi_i - \langle\phi\rangle$, $\Delta n_i = n_i - n_{\text{pre}}$, α and τ are dimensionless constants. τ represents the correlation between consecutive spike phases. Stronger correlations mean a smaller value of τ. η_i is the difference due to input jitter and intrinsic noise between the observed phase $\Delta\phi_{i+1}$ and the predicted value $\Delta\phi_i/\tau + \alpha\Delta n_i$. In the linear-map approximation it is replaced by a phenomenological noise source with variance σ_η^2.

The phenomenological constants α and τ were estimated using the procedure given in the appendix. For the map shown in figure 3(*b*), $\alpha = 0.0177$, $\tau = 3.70$, $\sigma_n = 19$ and $\sigma_\eta = 0.036$. Note that in terms of the parameters of the model simulations, the variance $\alpha^2\sigma_n^2$ varied as $\frac{1}{n_{\text{pre}}}$ and the variance σ_η^2 of η_i increased with both D and σ_{in}. The map describes how a given deviation of $\Delta\phi_i$ is driven back to the 'fixed point', $\Delta\phi = 0$, in the absence of input fluctuations, $\Delta n_i = 0$. The observed spike phase $\Delta\phi_{i+1}$ was close to the predicted value (figure 5(*a*); solid circles are the simulation results, squares are the linear-map approximation with $\eta_i = 0$). The difference η_i between the predicted and observed value was approximately normally distributed (figure 5(*b*)) and approximately uncorrelated between different cycles (figure 5(*c*)).

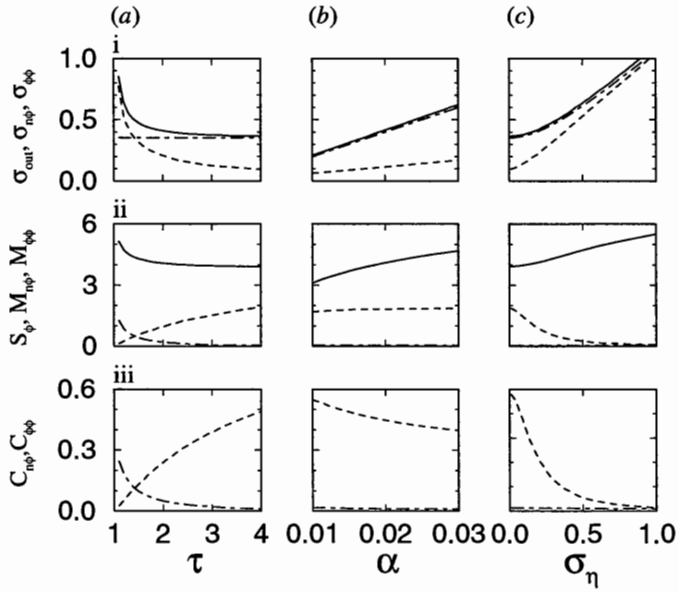

Figure 6. Information transmission in the linear-map approximation. The standard deviations σ, entropies S and coding fractions C are plotted as a function of (*a*) τ, (*b*) α and (*c*) σ_η. In each panel, i, σ_{out} (solid curves), $\sigma_{n\phi}$ (dashed curves) and $\sigma_{\phi\phi}$ (dot–dashed curves); ii, S_ϕ (solid curves), $M_{n\phi}$ (dashed curves) and $M_{\phi\phi}$ (dot–dashed curves); iii, $C_{n\phi}$ (dashed curves) and $C_{\phi\phi}$ (dot–dashed curves), were plotted. The map parameters were $\sigma_n = 20$, $\Delta = 0.1$, (*a*) $\alpha = 0.0177$ and $\sigma_\eta = 0.03$; (*b*) $\tau = 3.70$ and $\sigma_\eta = 0.03$; (*c*) $\alpha = 0.0177$ and $\tau = 3.70$.

The analytical predictions for the mutual information based on the linear map are derived in the appendix. The entropy S_ϕ (equation (10)), transmitted information $M_{n\phi}$ (equation (12)) and mutual information $M_{\phi\phi}$ (equation (13)) were expressed in terms of σ_{out} (the output jitter), $\sigma_{n\phi}$ (the jitter in $\Delta\phi_{i+1}$ conditional on n_i) and $\sigma_{\phi\phi}$ (the jitter in $\Delta\phi_{i+1}$ conditional on $\Delta\phi_i$). The coding fractions $C_{n\phi} = M_{n\phi}/S_\phi$ and $C_{\phi\phi} = M_{\phi\phi}/S_\phi$ were also determined. The above quantities were studied as a function of the linear-map parameters α, σ_η and τ. The results are shown in figure 6 and are summarized below.

The effect of correlations, τ. The variances σ^2_{out} and $\sigma^2_{n\phi}$ decreased with increasing τ, whereas $\sigma^2_{\phi\phi}$ was constant (figure 6(*a*)i). The output entropy S_ϕ and mutual information $M_{\phi\phi}$ also decreased with increasing τ (figure 6(*a*)ii). Since $\sigma_{n\phi}$ decreased faster with τ than σ_{out}, the transmitted information $M_{n\phi}$ increased with increasing τ (figure 6(*a*)ii). By the same token the coding fraction $C_{n\phi}$ increased, whereas $C_{\phi\phi}$ decreased with increasing τ (figure 6(*a*)iii). Consecutive phases are less correlated for higher τ values. Therefore, in the linear-map approximation information transmission increased when phase correlations decreased.

Signal size α. The variances σ^2_{out}, $\sigma^2_{n\phi}$ and $\sigma^2_{\phi\phi}$ all increased with increasing α when σ_n was kept constant (figure 6(*b*)i). The output entropy S_ϕ and transmitted information $M_{n\phi}$ also increased with increasing α, whereas $M_{\phi\phi}$ remained constant (figure 6(*b*)ii). The coding fractions $C_{n\phi}$ and $C_{\phi\phi}$ both decreased with increasing α (figure 6(*b*)iii). As mentioned before, $\alpha\sigma_n \sim 1/\sqrt{n_{pre}}$. Increasing the biophysical size of the signal, α, increased the absolute amount of transmitted information, but not necessarily the efficiency as measured by the coding fraction.

The effect of noise, σ_η. The variances σ^2_{out}, $\sigma^2_{n\phi}$ and $\sigma^2_{\phi\phi}$ all increased with increasing σ_η (figure 6(*c*)i). As a result the output entropy S_ϕ increased, the transmitted information $M_{n\phi}$ decreased and $M_{\phi\phi}$ remained constant with increasing noise strength σ_η (figure 6(*c*)ii). The coding fractions $C_{n\phi}$ and $C_{\phi\phi}$ both decreased with increasing σ_η (figure 6(*c*)iii). Noise therefore decreased the amount of transmitted information, as expected.

3.5. Experimental results

The information-theoretical analysis was applied to experimental data from rat prefrontal cortex and hippocampal neurons recorded *in vitro*. A current waveform was injected in the soma to mimic the synaptic inputs generated by a synchronized network of interneurons (figure 1(*b*) and methods). Briefly, presynaptic spike times were generated as in the model simulation. Each presynaptic spike induced a hyperpolarizing current pulse. The injected current was the sum of all hyperpolarizing pulses plus a depolarizing offset current to give the neuron maintained activity.

A representative intracellular voltage recording and the corresponding injected synaptic current for $\langle n_i \rangle = n_{\text{pre}} = 5$ are shown in figure 7(*a*)i and ii. For this input the relative fluctuations in n_i were large, approximately 44%. The neuron often skipped a cycle. However, when a neuron spiked it did so reliably in all 11 trials; it also reliably skipped the same cycles across different trials (figures 7(*a*)iii and iv). The precision was low, $\sigma_{\text{out}} = 4$ ms, and the phase histogram P_ϕ was broad (figure 7(*a*)v). The conditional average $\langle n \rangle$ of the number of input pulses increased monotonically with ϕ, since the larger the inhibition, the later the neuron fired (figure 7(*a*)vi). The mutual information was $M_{n\phi} \approx 1.27 \pm 0.23$ bits. There were correlations between consecutive spike phases observed in the ϕ_{i+1} versus ϕ_i scatter plot (figure 7(*a*)vii) and $M_{\phi\phi} = 0.64 \pm 0.48$ bits.

For a higher average presynaptic input frequency, $n_{\text{pre}} = 50$, the injected synaptic current and the intracellular voltage recording were more regular (figures 7(*b*)i and ii). The neuron rarely skipped cycles: only three out of 76 cycles (figure 7(*b*)i). The spiking was reliable (figures 7(*b*)iii and iv) and precise (figure 7(*b*)v). The output jitter, σ_{out}, was approximately equal to the input jitter, $\sigma_{\text{in}} = 1$ ms. The conditional average $\langle n \rangle$ increased linearly with ϕ (figure 7(*b*)vi). The consecutive spike phases were less correlated compared with $n_{\text{pre}} = 5$, with $M_{\phi\phi} = 0.16 \pm 0.06$ bits, and the scatterplot (figure 7(*b*)vii) had one compact cluster of data points.

The firing rate increased with n_{pre} towards the 1:1 entrained value of $f = 40$ Hz (figure 8(*a*)), while at the same time the output jitter was reduced to about 1 ms (figure 8(*b*)). The mutual information decreased with increasing n_{pre}, confirming the model prediction in figure 4(*b*). As the neuron became more entrained the correlations between consecutive spike phases were reduced, consistent with the results in figure 2(*b*)iv.

Based on figure 4(*b*), it was expected that $M_{n\phi}$ would increase with increasing n_{pre}, for small n_{pre}. In figure 8(*c*), there is a plateau for n_{pre} between 4 and 20, but no clear sign of an optimum value.

The above results were obtained by repeatedly injecting one time series corresponding to the presynaptic drive for a given n_{pre} value. The variance in f, σ_{out}, $M_{n\phi}$ and $M_{\phi\phi}$ across five different time series (figure 9) was determined using three different neurons. The firing rate was approximately the same for $n_{\text{pre}} = 10$ and $n_{\text{pre}} = 50$, though its value varied between different neurons (figure 9(*a*)). However, as before, σ_{out}, $M_{n\phi}$ and $M_{\phi\phi}$ decreased with n_{pre} (figures 9(*b*)–(*d*)). The standard deviation due to different time series was smaller than the estimated sampling error in two out of three neurons, but was larger in neuron 1 in figure 9. Thus, the results for one time series for the synaptic drive should be representative for the ensemble of possible time series within the sampling error.

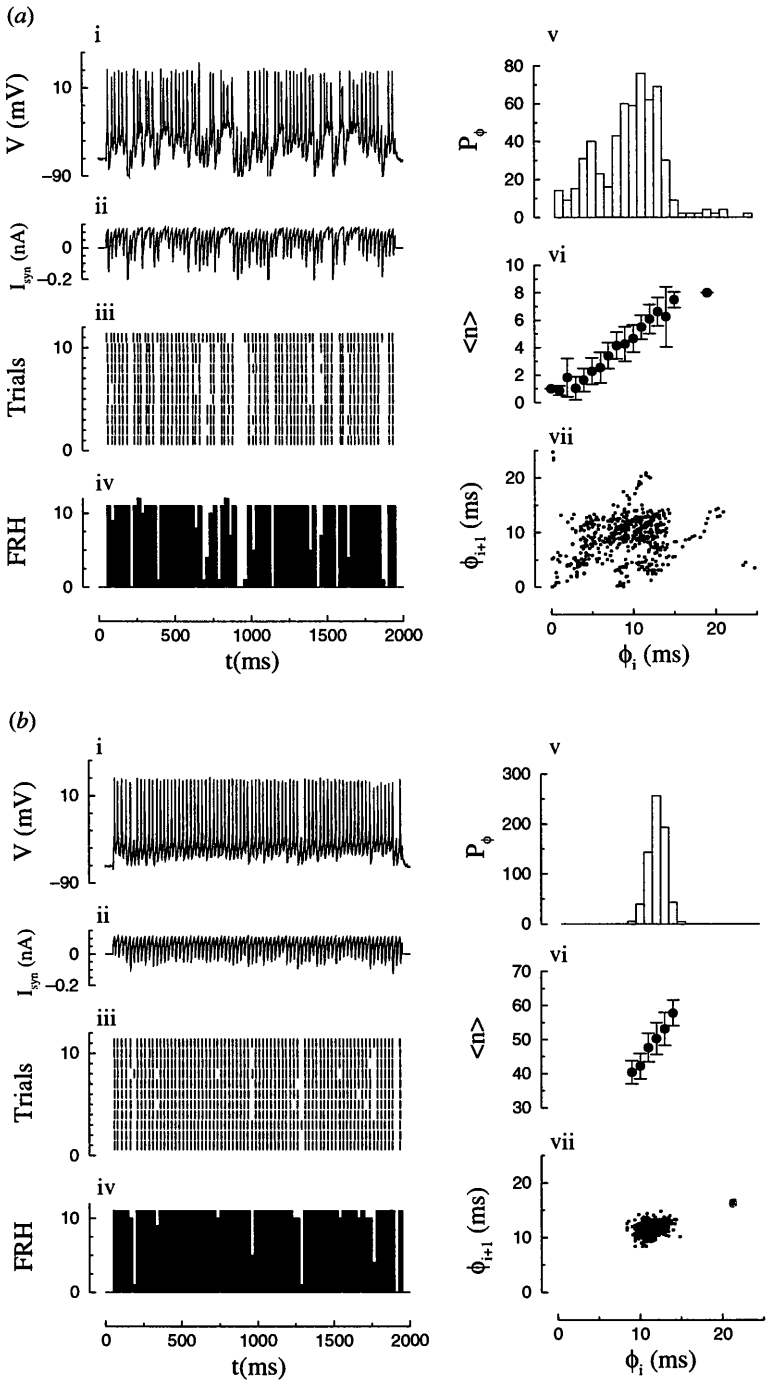

Figure 7. Regular spiking of a rat hippocampal interneuron driven by a simulated synaptic drive from a network of inhibitory interneurons firing at 40 Hz with input jitter $\sigma_{in} = 1$ ms, with (*a*) $n_{pre} = 5$ and (*b*) $n_{pre} = 50$. In each panel, i, intracellular voltage; ii, injected synaptic current divided by gain G; iii, rastergram; iv, firing rate histogram (FRH) versus time; v, phase histogram P_ϕ; vi, conditional average $\langle n \rangle$ versus phase ϕ, and vii, scatterplot of ϕ_{i+1} versus ϕ_i. Gain $G = 3$, current amplitude $A = 0.2$ nA, average current $a = 0.05$ nA (see methods).

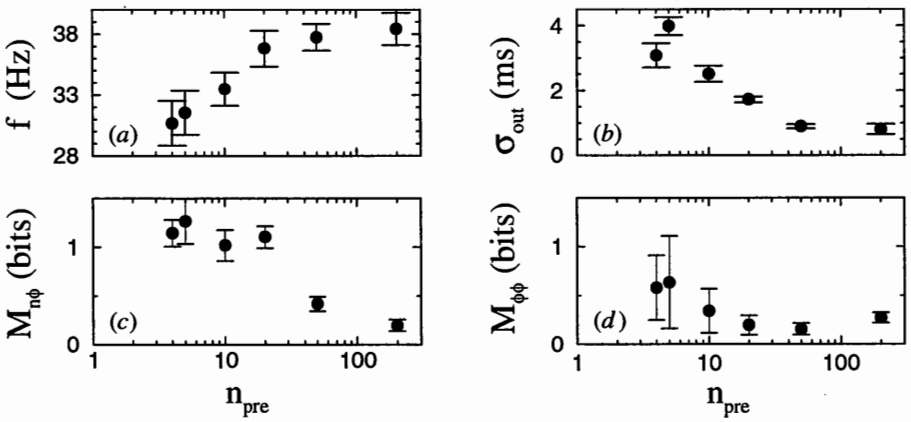

Figure 8. Summary statistics of the data from the hippocampal neuron shown in figure 7 over a wider range of n_{pre} values. (*a*) firing rate f, (*b*) output jitter σ_{out} and mutual information (*c*) $M_{n\phi}$ and (*d*) $M_{\phi\phi}$ as a function of the average number of pulses per cycle, n_{pre}. The error bars in (*a*) and (*b*) are the standard deviation across different trials; those in (*c*) and (*d*) represent the estimate of the sampling error. A transient of 200 ms was discarded before analysis; the bin width for the phase histogram was 1 ms.

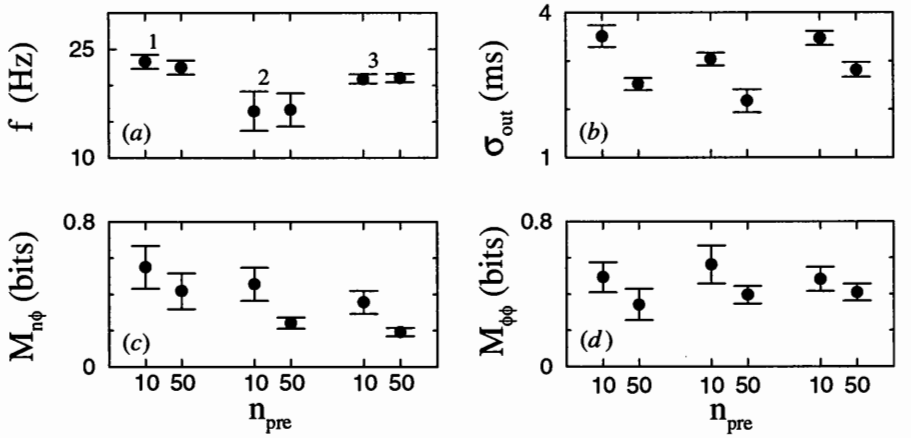

Figure 9. Variance in the measured quantities due to different patterns of current injection: (*a*) firing rate f, (*b*) output jitter σ_{out} and mutual information (*c*) $M_{n\phi}$ and (*d*) $M_{\phi\phi}$ for $n_{pre} = 10$ and 50. The error bars are the standard deviation over five different time series for the input synaptic drive. Results from three different neurons, labelled 1–3. A transient of 500 ms was discarded and the phase bin width was 2 ms. The gain G, amplitude A and average a of the current drive were 1, (G, A, a) = (4.5, 0.10 nA, 0.05 nA), 2, (2.0, 0.10 nA, 0.07 nA), 3, (1.5, 0.10 nA, 0.07 nA).

Interneurons could also be 1:1 entrained to a 20 Hz synaptic drive (figure 10). The neuron fired at 20 Hz for n_{pre} values between 5 and 200. There was a pronounced afterhyperpolarization following each action potential (figure 10(*a*)). The transmitted information was small, $M_{n\phi}$ was between 0.2 and 0.4 bits with an estimated sampling error of 0.2 bits, and the correlation between consecutive phases was large, $M_{\phi\phi}$ was between 1 bit and 1.5 bits with an estimated sampling error of 0.8 bits. The variation of the conditional average $\langle n \rangle$ versus ϕ was small compared with its standard deviation (shown as error bars in figure 10(*f*)). The ϕ_i versus ϕ_{i+1} plot (figure 10(*g*)) had an elongated shape compared with the compact cluster in figure 7(*b*)vii.

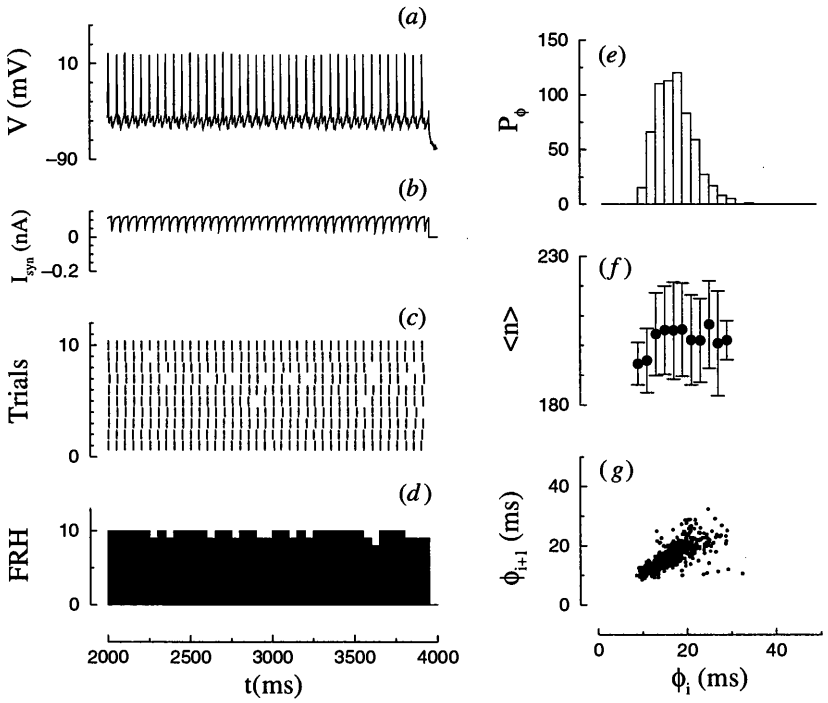

Figure 10. Dynamics of a hippocampal interneuron 1:1 entrained to a 20 Hz input current injection with gain $G = 3.0$, amplitude $A = 0.10$ nA, average $a = 0.07$ nA and $n_{\text{pre}} = 200$. The quantities plotted are as described in the caption to figure 7.

The time constant of the GABAergic inhibition, $t_i = 10$ ms, was too small compared with the interspike interval to determine the spike times with high precision. As a result the phase could precess from cycle to cycle, which yielded an increased output jitter that overwhelmed the signal-induced jitter. Similar results were obtained for two other neurons driven by a 10 Hz synaptic drive (not shown).

Interneurons could be entrained to a 40 Hz synaptic drive at ratios different from 1:1 (figure 11). The intracellular voltage recordings for $n_{\text{pre}} = 200$ were approximately periodic for $t > 1000$ ms; the neuron then produced two spikes per three cycles (figure 11(*a*)i). The conditional average $\langle n \rangle$ did not vary with ϕ within the standard deviation (figure 11(*a*)vi). The ϕ_{i+1} versus ϕ_i scatterplot consisted of two separate clusters (figure 11(*a*)vii); this deterministic structure yielded a non-zero value of $M_{\phi\phi}$ (figure 11(*b*)iv). The large correlations between consecutive spike phases were due to 2:3 entrainment and led to a large non-signal-related variance in the spike phase, which resulted in a low value of $M_{n\phi}$ (figure 11(*b*)iii). This is consistent with the model result outside 1:1 entrainment in figure 3(*c*). The output jitter was close to 2 ms for n_{pre} values between 5 and 200, while the firing rate increased from 26 to about 29 Hz (figure 11(*b*)i and ii). For these n_{pre}-values the transmitted information was small, $M_{n\phi} \approx 0.1$ bits, but $M_{\phi\phi}$ took values close to 0.5 bits per spike (figures 11(*b*)iii and iv).

Synaptic drives with an input jitter σ_{in} varying between 1 and 5 ms were injected into four different hippocampal interneurons and one in prefrontal cortex. 1:1, 1:2 and 2:3 entrainment was observed. Three out of five neurons had a pronounced depolarizing sag after a hyperpolarizing current pulse (possibly due to an h current) and therefore a transient of up to 1000 ms was discarded before analysis. During the transient neurons could be 1:1 entrained.

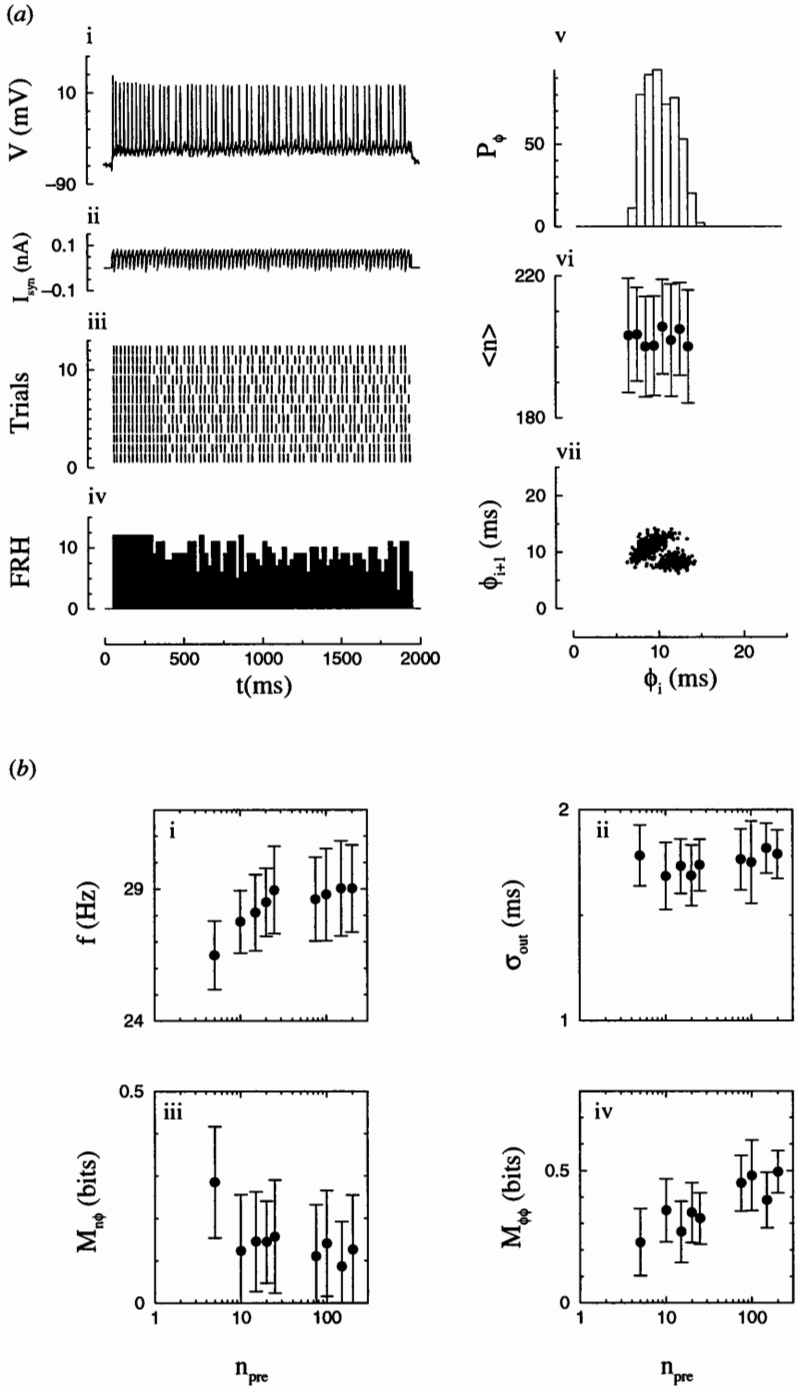

Figure 11. Dynamics of a hippocampal interneuron approximately 2:3 entrained to a 40 Hz input current injection with gain $G = 2.5$, $A = 0.10$ nA and $a = 0.07$ nA. (*a*) Results for $n_{pre} = 200$; the quantities plotted are as described in the caption to figure 7. (*b*) i, Firing rate f, ii, output jitter σ_{out}, and mutual information iii, $M_{n\phi}$, and iv, $M_{\phi\phi}$, were plotted as a function of the average number of pulses per cycle, n_{pre}. The error bars in i and ii were the standard deviation across different trials, those in iii and iv represented the estimated sampling error. A transient of 500 ms was discarded before analysis and the phase bin width was 1 ms.

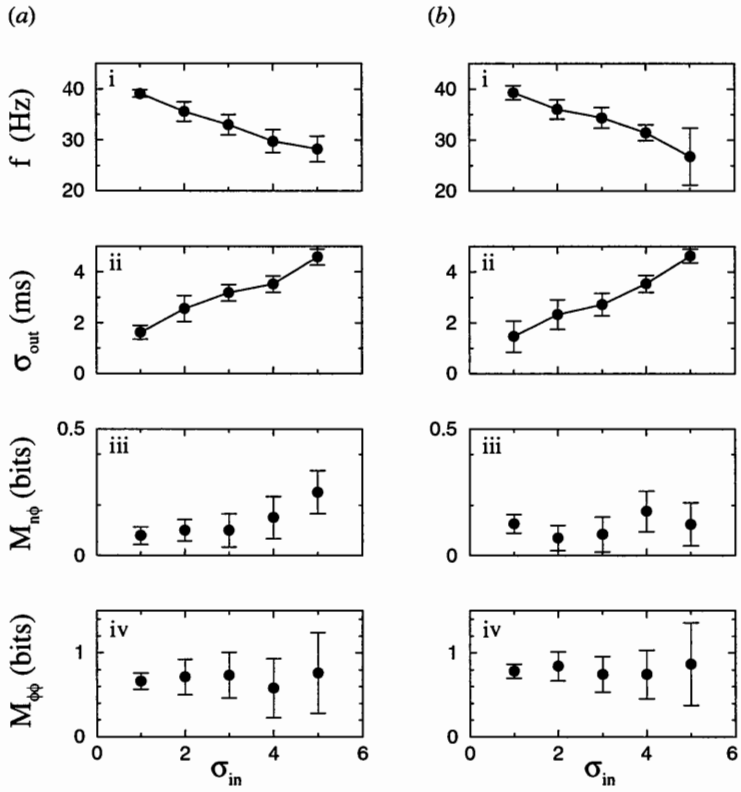

Figure 12. The input jitter decreases the firing rate and increases the output jitter in a prefrontal cortex interneuron. i, Firing rate f, ii, output jitter σ_{out}, and mutual information iii, $M_{n\phi}$, and iv, $M_{\phi\phi}$, as a function of the input jitter σ_{in} for (*a*) $n_{pre} = 10$ and (*b*) $n_{pre} = 20$. The error bars in i and ii were the standard deviation across the 17 trials; those in iii and iv represented the estimated sampling error. The transient was 200 ms, phase bin width was 3 ms, drive frequency was 40 Hz, the gain $G = 1.2$, amplitude $A = 0.1$ nA and average $a = 0.1$ nA.

Figure 12 shows the results for an 1:1 entrained interneuron in prefrontal cortex. The effective amplitude of the injected synaptic drive—the difference between maximum and minimum input current—decreased with increasing σ_{in}, but the tonic hyperpolarizing current increased. As a result, the firing rate decreased (figures 12(*a*)i and (*b*)i), whereas the output jitter increased (figures 12(*a*)ii and (*b*)ii) with σ_{in}. Similar results were found for the model (not shown). The transmitted information was small, $M_{n\phi} < 0.3$ bits, and $M_{\phi\phi}$ was between 0.6 and 1.0 bits. For $n_{pre} = 10$, $M_{n\phi}$ increased marginally with σ_{in} (figure 12(*a*)iii), whereas for $n_{pre} = 20$ it remained approximately constant (figure 12(*b*)iii). In both cases $M_{\phi\phi}$ remained constant, but the sampling error in $M_{\phi\phi}$ increased with σ_{in}.

4. Discussion

The goal of this study was to determine how well an entrained neuron can convey the number of inhibitory postsynaptic potentials in a cycle in the phase of the output spike. The output entropy is not a good indicator of the transmitted information. Indeed, outside 1:1 entrainment the output entropy is high and the mutual information is low, whereas during entrainment the output

entropy is small, but the mutual information has increased. The mutual information limits the maximum amount of information any postsynaptic neuron can infer about the presynaptic input to the emitting neuron. Off the entrainment step, the neuron has a high information capacity, but relatively little of it is about the emitting neuron's input. During entrainment, the emitting neuron produces a small amount of information, but most of it is 'useful'. The neuron can thus be in two states: one in which the phase variation from cycle to cycle reflects the variation in the input, and one in which the variation mostly reflects the internal correlations. Decreasing or increasing the current drive can switch the neuron from the entrained state to a non-entrained state.

During entrainment on the 1:1 step a neuron produces one spike per cycle of the input (Longtin and Chialvo 1998, Coombes and Bressloff 1999, Tiesinga and Sejnowski 2001) and the output jitter is reduced (Hunter *et al* 1998). If the goal is to transmit the period of the signal with high fidelity, then the output jitter, which represents the distortion of the signal, can be further reduced by reducing σ_{in} and increasing n_{pre}, leading to perfect transmission at $\sigma_{\text{in}} = 0$ and $n_{\text{pre}} \to \infty$. Therefore, for transmitting periodicity, entrainment and optimal signal transmission are equivalent. Here, however, the goal was to transmit information about the state of the inhibitory network driving the neuron. The periodicity of the presynaptic drive is the carrier wave and the signal is the presynaptic activity n_i. The output jitter contains the transmitted information and is not merely output noise. The mutual information between n and ϕ attains an optimal value at a finite value of n_{pre}. Increasing n_{pre} to large values would ultimately lead to zero information transmission (figure 4(*b*)). $M_{n\phi}$ also attains its optimum for non-zero σ_{in} when there are synaptic saturation effects. Therefore, optimal information transmission is not simply equivalent to being entrained, in contrast to the aforementioned task.

The model predictions were supported by *in vitro* experiments in cortex and hippocampus. First, neurons could be 1:1 entrained to a periodic synaptic input and could spike with higher precision compared with their input. Second, information transmission decreased with decreased input signal amplitude. Third, internal correlations and input spike-time jitter reduced information transmission.

There were also some differences between the model simulations and experiments. For zero intrinsic noise, the transmitted information increased in model simulations when the mutual information $M_{\phi\phi}$ decreased (figures 2(*b*)iii and iv). This relation was observed in experiment in figures 10 and 11, but not in figures 8 and 9. Two factors could potentially account for these differences. First, noise reduced the value of $M_{\phi\phi}$ (data not shown) and also reduced $M_{n\phi}$ (figure 4(*h*)). Hence, $M_{n\phi}$ and $M_{\phi\phi}$ depended on both correlations as well as noise levels. In model simulations and the linear-map approximation these two factors could be varied independently in order to delineate their effects. This was not possible in experiments since intrinsic noise could covary with changes in the injected current. Second, sampling errors were more difficult to control due to the small number of trials in experiment. This made comparison of the behaviour of $M_{n\phi}$ and $M_{\phi\phi}$ difficult.

The model neuron was driven by inhibitory conductance pulses, whereas in experiment the neuron was driven by an injected current that did not depend on the neuron's voltage. In preliminary experiments where periodic inhibitory conductance pulse trains were injected using dynamic clamp (Sharp *et al* 1993), neurons became entrained to the drive and transmitted information in their phase (data not shown). We did not make a detailed quantitative comparison between experiments with current injection and conductance injection to see whether this could account for some of the differences seen between experiment and model. Cortical neurons *in vivo* receive a barrage of excitatory and inhibitory synaptic inputs. Model simulations (Tiesinga *et al* 2000) and experiments using dynamic clamp (Destexhe *et al* 2001) indicate that the *in vivo* dynamics of the neuron is very different from that under *in vitro* conditions. Most of the experimental results reported here were for interneurons because it was easier

to 1:1 entrain them to a 40 Hz drive. This is consistent with recent results on the frequency preferences of interneurons compared with pyramidal cells (Fellous *et al* 2001, Protopapas and Bower 2001). Under *in vivo* conditions the membrane time constant of neurons is reduced. It is therefore possible that under these conditions pyramidal cells could become entrained to 40 Hz inhibition. However, it remains an open question how the reported effects on information transmission carry over to *in vivo* conditions.

Interneuron networks synchronize in the gamma frequency range between 30–80 Hz (Traub *et al* 1996a, Wang and Buzsáki 1996). We studied information transmission in the presence of synchronized inhibition at 40 Hz, but our results were robust against small changes in frequency (not shown). A key requisite in our study was that neurons could become entrained to the inhibitory drive. This occurred when the following three conditions were satisfied. First, the neuron should be depolarized enough in order to fire at approximately 40 Hz in the presence of inhibition. Second, the input frequency should be close to the inverse of the synaptic decay time constant (White *et al* 1998, Wang and Buzsáki 1996). Third, the noise strength should be small enough. Noise consisted of the input jitter σ_{in}, the variance σ_n^2 in the number of presynaptic pulses (the signal in our analysis), and intrinsic noise with strength D. In the model the driving current was important in determining whether a neuron would be entrained. The difference in entrainment behaviour between pyramidal cells and interneurons in experiment indicates that the membrane time constant and duration of the afterhyperpolarization may also be important factors. These issues are presently being addressed using more detailed biophysical models (Houweling *et al* 2001).

The model and experimental results presented here are related to earlier experimental results where a synchronized inhibitory synaptic drive was injected in cerebellar neurons using dynamic current clamp (Gauck and Jaeger 2000). However, in their case the synaptic strength was stronger than in our model. For stronger synapses in the model, we also reproduced their finding that increasing input jitter could reduce the firing rate (José *et al* 2001).

The temporal jitter in the discharge of LGN neurons can be as low as 0.6 ms (Reinagel and Reid 2000). The mutual information between input and output increased with decreasing temporal resolution up to 0.6 ms and could reach values as high as three to four bits per spike with $C_{n\phi} \approx 0.5$ (Reinagel and Reid 2000). This is comparable to our values of one to two bits per spike with $C_{n\phi} \sim 0.6$, for a bin width of 1 ms on the entrainment step. The estimate for the transmitted information could increase by 25% when the mutual information between the input and patterns consisting of multiple bins was calculated (Reinagel and Reid 2000; see also Brenner *et al* 2000, Eguia *et al* 2000, Tiesinga 2001, Chacron *et al* 2001). In our model, entrainment enhances information transmission by making spike phases more independent. Therefore, considering multiple consecutive phases instead of a single phase would not increase the mutual information. During entrainment each spike phase yields within one cycle an estimate for the input, and there is no need to wait for more cycles to complete the estimate.

In the bee and locust olfactory systems, Laurent and co-workers have shown that different odours activate overlapping ensembles of projection neurons (Laurent and Davidowitz 1994). The 20 Hz periodic discharge of the ensembles is coherent on a cycle-by-cycle basis and information about the odour is contained in the temporal firing pattern of projection neurons (Wehr and Laurent 1996). Synchronization of the projection neurons can be abolished by applying picrotoxin without changing the low-frequency temporal pattern (MacLeod and Laurent 1996). This desynchronization was shown to impair the ability of bees to distinguish two closely related odours (Stopfer *et al* 1997), and subsequently a population of neurons was found that was sensitive to the synchronization of projection neurons (MacLeod and Laurent 1998). The ability of the population to distinguish between two similar odours, based on their

spike trains, was reduced following desynchronization. A dynamical model of the antennal lobe based on Hodgkin–Huxley-type neurons reproduced these observations and demonstrated how synchronization can improve the odour discrimination of the network (Bazhenov *et al* 2001a, 2001b).

Tonic activation of local interneuron networks in hippocampal slices produces a synchronous inhibitory synaptic drive to pyramidal cells in the gamma frequency range (Whittington *et al* 1995, Wang and Buzsáki 1996, Traub *et al* 1996a, White *et al* 1998, Tiesinga and José 2000, Tiesinga *et al* 2001a). These interneuron networks may also be responsible for the long-range coherence of gamma oscillations (Traub *et al* 1996b). The same mechanism can generate gamma oscillations in cortical networks (Bush and Sejnowski 1996). It has been proposed that interneuron networks provide a clock signal to cortical principal cells, with the information embedded in the temporal sequence of action potentials (Buzsáki and Chrobak 1995). During entrainment the output phase of the neuron is more sensitive to small changes in the input. Here, we investigated the situation when both periodicity as well as the signal was in the inhibitory drive. However, the same sensitivity of output phase is present in response to small changes in excitatory inputs. Hence, the results reported here may be more widely applicable. In particular, entrainment to periodic synchronized inhibition could also facilitate information transmission between excitatory neurons.

Subcortical projections originating in the basal nucleus of the forebrain release the neuromodulator acetylcholine (ACh) in cortex. This projection is active during wakefulness and is reduced during slow-wave sleep. The ACh concentration thus varies between a high level during waking, and a low level during sleep. The known physiological effects of ACh include blockade of the slow afterhyperpolarization current (AHP), and an increased excitability (Madison *et al* 1987). Application of cholinergic agonists can induce synchronized gamma-frequency oscillations in hippocampal slices (Fisahn *et al* 1998, Fellous and Sejnowski 2000, Tiesinga *et al* 2001a). In our model neuron a higher ACh concentration corresponds to a higher driving current, making the neuron more excitable, switching the model neuron from a non-entrained to an entrained state. The information flow in cortex could therefore be dynamically gated by neuromodulators released by ascending subcortical projections.

These results point toward a new view of cortical information processing. Without entrainment a cortical neuron is a traditional integrator and transmits information through changes in its firing rate; during entrainment, which is promoted by neuromodulators and characterized by gamma band activity, a cortical neuron can transmit information about its inputs more efficiently by the relative spike timing within the cycle, as suggested by Hopfield (1995). In particular, the synchronized firing of cortical neurons in the 30–80 Hz range could represent conditions similar to the one studied here where information in the inhibitory pool can be efficiently encoded by the phases of pyramidal neurons. Experiments *in vivo* need to be carried out to test this possibility.

Acknowledgments

This work was partially funded by the Northeastern University CIRCS fund and by the National Science Foundation under grant no PHY99-07949 (JVJ), the Sloan-Swartz Center for Theoretical Neurobiology (PT) and Howard Hughes Medical Institute (JMF, TJS). Part of the calculation was performed at Northeastern University High Performance computer center. We thank Alexei Koulakov for useful suggestions. We thank the anonymous referees for comments that have improved the paper.

Appendix

Mutual information of linear map

We analysed the dynamics of the linear map in equation (3),

$$\Delta\phi_{i+1} = \frac{1}{\tau}\Delta\phi_i + \alpha\Delta n_i + \eta_i. \tag{4}$$

The parameters of this map were estimated by minimizing

$$\sigma_\eta^2 = \left\langle \left(\Delta\phi_{i+1} - \frac{1}{\tau}\Delta\phi_i - \alpha\Delta n_i \right)^2 \right\rangle,$$

using the data in figure 3(*b*) (the average $\langle\cdot\rangle$ is over all cycles i). This yielded the following expressions for α and τ:

$$\alpha = \frac{C_4C_3 - C_1C_5}{C_3^2 - C_1C_2}$$

$$\tau = \frac{C_1}{C_4 - C_3\alpha},$$

where $C_1 = \langle\Delta\phi_i^2\rangle = \langle\Delta\phi_{i+1}^2\rangle$, $C_2 = \langle\Delta n_i^2\rangle$, $C_3 = \langle\Delta n_i\Delta\phi_i\rangle$, $C_4 = \langle\Delta\phi_i\Delta\phi_{i+1}\rangle$, $C_5 = \langle\Delta n_i\Delta\phi_{i+1}\rangle$ and the bracket $\langle\cdot\rangle$ denotes a sum over all cycles i.

The output jitter was determined using the approximation that $\Delta\phi_i$ and Δn_i are continuous variables that take values between $-\infty$ and ∞ and that their dynamics is given by equation (4). Furthermore, it was assumed that the inputs Δn_i and η_i are normally distributed with zero mean and the variances are equal to σ_n^2 and σ_η^2, respectively. The solution to equation (4) can be obtained explicitly since it is linear and it is

$$\Delta\phi_{m+1} = \left(\frac{1}{\tau}\right)^m \Delta\phi_1 + \sum_{i=1}^{m} \left(\frac{1}{\tau}\right)^{m-i} (\alpha\Delta n_i + \eta_i). \tag{5}$$

The first term goes to zero in the limit $m \to \infty$. The second term is a sum of independent Gaussian variables, hence the sum itself is given by a set of Gaussian variables and the output jitter is

$$\sigma_{\text{out}}^2 = \langle\Delta\phi_\infty^2\rangle = \left[\sum_{i=0}^{\infty}\left(\frac{1}{\tau^2}\right)^i\right](\alpha^2\sigma_n^2 + \sigma_\eta^2) = \left(\frac{1}{1-\frac{1}{\tau^2}}\right)(\alpha^2\sigma_n^2 + \sigma_\eta^2). \tag{6}$$

The same result is obtained starting from a distribution of initial values $\Delta\phi_0$ and iterating equation (4). The distribution of $\Delta\phi_m$ will converge to a stationary distribution for large enough m, hence

$$\sigma_{\text{out}}^2 = \langle\Delta\phi_m^2\rangle = \langle\Delta\phi_{m+1}^2\rangle, \tag{7}$$

whereas from equation (4),

$$\langle\Delta\phi_{m+1}^2\rangle = \langle\Delta\phi_m^2\rangle/\tau^2 + \alpha^2\sigma_n^2 + \sigma_\eta^2, \tag{8}$$

which again in the limit $m \to \infty$ yields

$$\sigma_{\text{out}}^2 = \frac{\sigma_\eta^2 + \alpha^2\sigma_n^2}{1-\frac{1}{\tau^2}}. \tag{9}$$

Here $\langle\cdot\rangle$ denotes the average over initial condition $\Delta\phi_0$, noise η and input Δn. Equation (4) was iterated numerically for 1000 different initial values that were randomly drawn from a

normal distribution with unit variance, using the map parameters of figure 5. The ensemble variance converged within ten iterations to the σ_{out} given by equation (9) (data not shown).

Next, the mutual informations $M_{n\phi}$ and $M_{\phi\phi}$ were determined. The entropy of P_ϕ is (Rieke *et al* 1997)

$$S_\phi = \frac{1}{2}\log_2 2\pi e\frac{\sigma_{\text{out}}^2}{\Delta^2} = \log_2 \frac{\sigma_{\text{out}}}{\bar{\Delta}}. \tag{10}$$

Here Δ is the measurement scale. For jitter σ_{out} smaller than $\bar{\Delta} = \Delta/\sqrt{2\pi e}$ the entropy is zero because almost all measurements would fall into one bin. Δ is approximately given by the minimal phase difference that can be biophysically resolved. Here Δ was equal to the bin width of 1 ms. The mutual information is

$$M_{n\phi} = -\int \mathrm{d}\Delta\phi_{i+1} P(\Delta\phi_{i+1}) \log_2 P(\Delta\phi_{i+1}) + \int \mathrm{d}\Delta n_i P(\Delta n_i) \int \mathrm{d}\Delta\phi_{i+1} P(\Delta\phi_{i+1}|\Delta n_i) \log_2 P(\Delta\phi_{i+1}|\Delta n_i). \tag{11}$$

For simplicity, the symbol P is used to denote probability distributions, and the particular distribution is indicated by the argument: $P(\Delta n_i)$ is the distribution of Δn_i, $P(\Delta\phi_{i+1})$ is the distribution of $\Delta\phi_{i+1}$ and $P(\Delta\phi_{i+1}|\Delta n_i)$ is the distribution of $\Delta\phi_{i+1}$ conditional on Δn_i. For a fixed value of Δn_i, $\Delta\phi_{i+1}$ is equal to $\alpha\Delta n_i$ plus the sum of two Gaussian variables. The variance $\sigma_{n\phi}^2$ of their sum is $\sigma_{\text{out}}^2/\tau^2 + \sigma_\eta^2$. Thus the conditional distribution $P(\Delta\phi_{i+1}|\Delta n_i)$ is a Gaussian, and its entropy is independent of Δn_i, yielding

$$M_{n\phi} = \log_2 \frac{\sigma_{\text{out}}}{\bar{\Delta}} - \log_2 \frac{\sigma_{n\phi}}{\bar{\Delta}} = \log_2 \frac{\sigma_{\text{out}}}{\sigma_{n\phi}} = \frac{1}{2}\log_2 \frac{\tau^2}{1 + \left(1 - \frac{1}{\tau^2}\right)\left(1 + \frac{\alpha^2\sigma_n^2}{\sigma_\eta^2}\right)^{-1}}. \tag{12}$$

For a fixed value of $\Delta\phi_i$, $\Delta\phi_{i+1} = \frac{1}{\tau}\Delta\phi_i$ plus a sum of Gaussians with a total variance $\sigma_{\phi\phi}$ equal to $\alpha^2\sigma_n^2 + \sigma_\eta^2$. The mutual information is, as before,

$$M_{\phi\phi} = \log_2 \frac{\sigma_{\text{out}}}{\sigma_{\phi\phi}} = -\frac{1}{2}\log_2\left(1 - \frac{1}{\tau^2}\right). \tag{13}$$

The coding fractions are defined as $C_{n\phi} = M_{n\phi}/S_\phi$ and $C_{\phi\phi} = M_{\phi\phi}/S_\phi$.

The above expressions for $M_{n\phi}$ and $M_{\phi\phi}$ are only valid when the entropy of $P(\Delta\phi_i)$, $P(\Delta\phi_{i+1}|\Delta n_i)$ and $P(\Delta\phi_{i+1}|\Delta\phi_i)$ is positive. This leads to the constraints $\sigma_{\text{out}} > \bar{\Delta}$, $\sigma_{n\phi} > \bar{\Delta}$ and $\sigma_{\phi\phi} > \bar{\Delta}$, yielding

$$\left(\alpha^2\sigma_n^2 + \sigma_\eta^2\right) \Big/ \left(1 - \frac{1}{\tau^2}\right) \geqslant \bar{\Delta}^2, \tag{14}$$

$$\sigma_n^2 \frac{\alpha^2}{\tau^2 - 1} + \sigma_\eta^2 \frac{\tau^2}{\tau^2 - 1} \geqslant \bar{\Delta}^2, \tag{15}$$

$$\alpha^2\sigma_n^2 + \sigma_\eta^2 \geqslant \bar{\Delta}^2. \tag{16}$$

For small $\alpha\sigma_n$ and σ_η these inequalities may not hold and the following results are obtained. $M_{n\phi} = 0$ when $\sigma_{\text{out}} < \bar{\Delta}$ and $\sigma_{n\phi} < \bar{\Delta}$, and $C_{n\phi}$ was defined as zero. When $\sigma_{\text{out}} > \bar{\Delta}$ and $\sigma_{n\phi} < \bar{\Delta}$, $M_{n\phi} = S_\phi$ and $C_{n\phi} = 1$. The behaviour of $M_{n\phi}$ and $C_{n\phi}$ is shown in figure A.1 as a function of σ_η for values of the variance close to $\bar{\Delta}$. The mutual information $M_{n\phi}$ was zero for $\sigma_\eta \leqslant 0.2$, then became non-zero, after which it decreased with increasing σ_η (figure A.1(*b*)). Concomitantly, the coding fraction $C_{n\phi}$ jumped from zero to one, and then decreased with increasing σ_η (figure A.1(*c*)). There is optimal information transfer near $\sigma_\eta \approx 0.2$. The above result shows how important it is to match the value of Δ to the relevant biophysical scale. Otherwise, spurious resonances may be obtained.

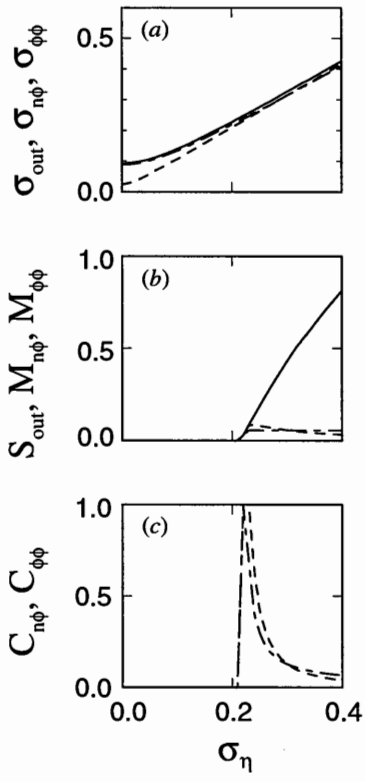

Figure A.1. The value of the bin width Δ can affect the measured information transfer. (*a*) σ_{out} (solid curves), $\sigma_{n\phi}$ (dashed curves) and $\sigma_{\phi\phi}$ (dot–dashed curves); (*b*) S_ϕ (solid curves), $M_{n\phi}$ (dashed curves) and $M_{\phi\phi}$ (dot–dashed curves); (*c*) $C_{n\phi}$ (dashed curves) and $C_{\phi\phi}$ (dot–dashed curves), were plotted as a function of the noise standard deviation σ_η. The map parameters were $\alpha = 0.0177, \tau = 3.70, \sigma_n = 5$ and $\Delta = 1$.

Neuron model

The equation for the membrane potential of the neuron studied was

$$C_m \frac{\mathrm{d}V}{\mathrm{d}t} = -I_{\text{Na}} - I_{\text{K}} - I_L - I_{\text{syn}} + I_0 + C_m \xi, \tag{17}$$

with the leak current $I_L = g_L(V - E_L)$, the sodium current $I_{\text{Na}} = g_{\text{Na}} m_\infty^3 h(V - E_{\text{Na}})$, the potassium current $I_{\text{K}} = g_{\text{K}} n^4 (V - E_K)$ and the synaptic current I_{syn} as described in the methods. The intrinsic noise ξ has zero mean and variance $2D$, and I_0 is the tonic drive. The channel kinetics are given in terms of m, n and h. They satisfy the following first-order kinetic equations:

$$\frac{\mathrm{d}x}{\mathrm{d}t} = \zeta(\alpha_x(1 - x) - \beta_x x). \tag{18}$$

Here x labels the different kinetic variables m, n and h, and $\zeta = 5$ is a dimensionless timescale that can be used to tune the temperature-dependent speed with which the channels open or close. The rate constants are (Wang and Buzsáki 1996)

$$\begin{aligned}
\alpha_m &= \frac{-0.1(V + 35)}{\exp(-0.1(V + 35)) - 1}, \\
\beta_m &= 4\exp(-(V + 60)/18), \\
\alpha_h &= 0.07\exp(-(V + 58)/20), \\
\beta_h &= \frac{1}{\exp(-0.1(V + 28)) + 1},
\end{aligned}$$

$$\alpha_n = \frac{-0.01(V+34)}{\exp(-0.1(V+34))-1},$$
$$\beta_n = 0.125\ \exp(-(V+44)/80).$$

We make the approximation that m takes the asymptotic value $m_\infty(V(t)) = \alpha_m/(\alpha_m + \beta_m)$ instantaneously. The standard set of values for the conductances used in this paper are $g_{\mathrm{Na}} = 35$, $g_{\mathrm{K}} = 9$ and $g_L = 0.1$ (in mS cm^{-2}), and we have taken $E_{\mathrm{Na}} = 55$ mV, $E_{\mathrm{K}} = -90$ mV and $E_L = -65$ mV. The membrane capacitance is $C_m = 1\ \mu$F cm^{-2}.

The resulting equations with noise are integrated using an adapted second-order Runge–Kutta method (Greenside and Helfand 1981) implemented in a Fortran program, with time step $\mathrm{d}t = 0.01$ ms. The accuracy of this integration method was checked for the dynamical equations without noise ($D = 0$) by varying $\mathrm{d}t$ and comparing the result with the one obtained with the standard fourth-order Runge–Kutta method (Press *et al* 1992) with a time-step $\mathrm{d}t$ of 0.05 ms.

References

Bair W 1999 Spike timing in the mammalian visual system *Curr. Opin. Neurobiol.* **9** 447–53

Bazhenov M, Stopfer M, Rabinovich M, Abarbanel H, Sejnowski T and Laurent G 2001a Model of cellular and network mechanisms for odor-evoked temporal patterning in the locust antennal lobe *Neuron* **30** 569–81

Bazhenov M, Stopfer M, Rabinovich M, Huerta R, Abarbanel H, Sejnowski T and Laurent G 2001b Model of transient oscillatory synchronization in the locust antennal lobe *Neuron* **30** 553–67

Beierlein M, Gibson J and Connors B 2000 A network of electrically coupled interneurons drives synchronized inhibition in neocortex *Nat. Neurosci.* **3** 904–10

Berry M and Meister M 1998 Refractoriness and neural precision *J. Neurosci.* **18** 2200–11

Berry M, Warland D and Meister M 1997 The structure and precision of retinal spike trains *Proc. Natl Acad. Sci. USA* **94** 5411–16

Borst A and Theunissen F 1999 Information theory and neural coding *Nat. Neurosci.* **2** 947–57

Brenner N, Strong S, Koberle R, Bialek W and de Ruyter van Steveninck R 2000 Synergy in a neural code *Neural. Comput.* **12** 1531–52

Buracas G and Albright T 1999 Gauging sensory representations in the brain *Trends Neurosci.* **22** 303–9

Buracas G, Zador A, DeWeese M and Albright T 1998 Efficient discrimination of temporal patterns by motion-sensitive neurons in primate visual cortex *Neuron* **20** 959–69

Burkitt A and Clark G 1999 Analysis of integrate-and-fire neurons: synchronization of synaptic input and spike output *Neural. Comput.* **11** 871–901

Burkitt A and Clark G 2000 Analysis of synchronization in the response of neurons to noisy synaptic input *Neurocomputing* **32–33** 67–75

Bush P and Sejnowski T 1996 Inhibition synchronizes sparsely connected cortical neurons within and between columns in realistic network models *J. Comput. Neurosci.* **3** 91–110

Buzsáki G and Chrobak J 1995 Temporal structure in spatially organized neuronal ensembles: a role for interneuronal networks *Curr. Opin. Neurobiol.* **5** 504–10

Cecchi G, Sigman M, Alonso J, Martinez L, Chialvo D and Magnasco M 2000 Noise in neurons is message dependent *Proc. Natl Acad. Sci. USA* **97** 5557–61

Chacron M, Longtin A and Maler L 2001 Negative interspike interval correlations increase the neuronal capacity for encoding time-dependent stimuli *J. Neurosci.* **21** 5328–43

Cobb S, Buhl E, Halasy K, Paulsen O and Somogyi P 1995 Synchronization of neuronal activity in hippocampus by individual GABAergic interneurons *Nature* **378** 75–78

Coombes S and Bressloff P 1999 Mode locking and Arnold tongues in integrate-and-fire neural oscillators *Phys. Rev.* E **60** 2086–96

Cover T and Thomas J 1991 *Elements of Information Theory* (New York: Wiley)

Deans M, Gibson J, Sellitto C, Connors B and Paul D 2001 Synchronous activity of inhibitory networks in neocortex requires electrical synapses containing connexin36 *Neuron* **31** 477–85

de Ruyter van Steveninck R, Lewen G, Strong S, Koberle R and Bialek W 1997 Reproducibility and variability in neural spike trains *Science* **275** 1805–8

Destexhe A, Rudolph M, Fellous J-M and Sejnowski T 2001 Fluctuating synaptic conductances recreate *in vivo*-like activity in neocortical neurons *Neuroscience* at press

Eguia M, Rabinovich M and Abarbanel H 2000 Information transmission and recovery in neural communications channels *Phys. Rev.* E **62** 7111–22

Fellous J-M, Houweling A, Modi R, Rao R, Tiesinga P and Sejnowski T 2001 The frequency dependence of spike timing reliability in cortical pyramidal cells and interneurons *J. Neurophys.* **85** 1782–7

Fellous J-M and Sejnowski T 2000 Cholinergic induction of oscillations in the hippocampal slice in the slow (0.5–2 Hz), theta (5–12 Hz) and gamma (35–70 Hz) bands *Hippocampus* **10** 187–97

Fisahn A, Pike F, Buhl E and Paulsen O 1998 Cholinergic induction of network oscillations at 40 Hz in the hippocampus *in vitro Nature* **394** 186–9

Galarreta M and Hestrin S 1999 A network of fast-spiking cells in the neocortex connected by electrical synapses *Nature* **402** 72–5

Galarreta M and Hestrin S 2001a Electrical synapses between GABA-releasing interneurons *Nat. Rev. Neurosci.* **2** 425–33

Galarreta M and Hestrin S 2001b Spike transmission and synchrony detection in networks of GABAergic interneurons *Science* **292** 2295–9

Gauck V and Jaeger D 2000 The control of rate and timing of spikes in the deep cerebellar nuclei by inhibition *J. Neurosci.* **20** 3006–16

Gerstner W, Kempter R, van Hemmen J and Wagner H 1996 A neuronal learning rule for sub-millisecond temporal coding *Nature* **383** 76–81

Gibson J, Beierlein M and Connors B 1999 Two networks of electrically coupled inhibitory neurons in neocortex *Nature* **402** 75–9

Greenside H and Helfand E 1981 Numerical integration of stochastic differential equations *Bell Syst. Tech. J.* **60** 19–27

Gur M, Beylin A and Snodderly D 1997 Response variability of neurons in primary visual cortex (V1) of alert monkeys *J. Neurosci.* **17** 2914–20

Harsch A and Robinson H 2000 Postsynaptic variability of firing in rat cortical neurons: the roles of input synchronization and synaptic NMDA receptor conductance *J. Neurosci.* **20** 6182–92

Hopfield J 1995 Pattern recognition computation using action potential timing for stimulus representation *Nature* **376** 33–6

Hormuzdi S, Pais I, LeBeau F, Towers S, Rozov A, Buhl E, Whittington M and Monyer H 2001 Impaired electrical signaling disrupts gamma frequency oscillations in connexin 36-deficient mice *Neuron* **31** 487–95

Houweling A, Modi R, Ganter P, Fellous J and Sejnowski T 2001 Models of frequency preferences of prefrontal cortical neurons *Neurocomputing* **38–40** 231–8

Hunter J, Milton J, Thomas P and Cowan J 1998 Resonance effect for neural spike time reliability *J. Neurophysiol.* **80** 1427–38

Jaeger D and Bower J 1999 Synaptic control of spiking in cerebellar Purkinje cells: dynamic current clamp based on model conductances *J. Neurosci.* **19** 6090–101

José J, Tiesinga P, Fellous J-M, Salinas E and Sejnowski T 2001 Synchronization as a mechanism for attentional modulation *Soc. Neurosci. Abstr.* **27** 722.11

Kempter R, Gerstner W, van Hemmen J and Wagner H 1998 Extracting oscillations. Neuronal coincidence detection with noisy periodic spike input *Neural. Comput.* **10** 1987–2017

Kistler W and van Hemmen J 1999 Delayed reverberation through time windows as a key to cerebellar function *Biol. Cybern.* **81** 373–80

Koos T and Tepper J 1999 Inhibitory control of neostriatal projection neurons by GABAergic interneurons *Nat. Neurosci.* **2** 467–72

Laurent G and Davidowitz H 1994 Encoding of olfactory information with oscillating neural assemblies *Science* **265** 1872–5

Longtin A and Chialvo D 1998 Stochastic and deterministic resonances for excitable systems *Phys. Rev. Lett.* **81** 4012–5

Lytton W and Sejnowski T 1991 Simulations of cortical pyramidal neurons synchronized by inhibitory interneurons *J. Neurophys.* **66** 1059–79

MacLeod K and Laurent G 1996 Distinct mechanisms for synchronization and temporal patterning of odor-encoding neural assemblies *Science* **274** 976–9

MacLeod K and Laurent G 1998 Who reads temporal information contained across synchronized and oscillatory spike trains *Nature* **395** 693–8

Madison D, Lancaster B and Nicoll R 1987 Voltage clamp analysis of cholinergic action in the hippocampus *J. Neurosci.* **7** 733–41

Mainen Z and Sejnowski T 1995 Reliability of spike timing in neocortical neurons *Science* **268** 1503–6

McCormick D, Connors B, Lighthall J and Prince D 1985 Comparative electrophysiology of pyramidal and sparsely spiny stellate neurons of the neocortex *J. Neurophys.* **54** 782–806

Nowak L, Sanchez-Vives M and McCormick D 1997 Influence of low and high frequency inputs on spike timing in visual cortical neurons *Cereb. Cortex* **7** 487–501

Oram M, Wiener M, Lestienne R and Richmond B 1999 Stochastic nature of precisely timed spike patterns in visual system neuronal responses *J. Neurophysiol.* **81** 3021–33

Press W, Teukolsky S, Vetterling W T and Flannery B P 1992 *Numerical Recipes* (Cambridge: Cambridge University Press)

Protopapas A and Bower J 2001 Spike coding in pyramidal cells of the piriform cortex of rat *J. Neurophys.* **86** 1504–10

Reich D, Victor J, Knight B, Ozaki T and Kaplan E 1997 Response variability and timing precision of neuronal spike trains *in vivo J. Neurophysiol.* **77** 2836–41

Reinagel P, Godwin D, Sherman S and Koch C 1999 Encoding of visual information by LGN bursts *J. Neurophysiol.* **81** 2558–69

Reinagel P and Reid R 2000 Temporal coding of visual information in the thalamus *J. Neurosci.* **20** 5392–400

Rieke F, Warland D, de Ruyter van Steveninck R R and Bialek W 1997 *Spikes: Exploring the Neural Code* (Cambridge, MA: MIT Press)

Salinas E and Sejnowski T 2000 Impact of correlated synaptic input on output variability in simple neuronal models *J. Neurosci.* **20** 6193–209

Shadlen M and Newsome W 1994 Noise, neural codes, and cortical organization *Curr. Opin. Neurobiol.* **4** 569–79

Shadlen M and Newsome W 1998 The variable discharge of cortical neurons: implications for connectivity, computation, and information coding *J. Neurosci.* **18** 3870–96

Shannon C and Weaver W 1949 *The Mathematical Theory of Communication* (Urbana, IL: University of Illinois Press)

Sharp A, O'Neil M, Abbott L and Marder E 1993 Dynamic clamp: computer-generated conductances in real neurons *J. Neurophysiol.* **69** 992–5

Softky W 1995 Simple codes versus efficient codes *Curr. Opin. Neurobiol.* **5** 239–47

Stevens C and Zador A 1998 Input synchrony and the irregular firing of cortical neuron *Nat. Neurosci.* **1** 210–17

Stopfer M, Bhagavan S, Smith B and Laurent G 1997 Impaired odor discrimination on desynchronization of odor-encoding neural assemblies *Nature* **390** 70–4

Tamas G, Buhl E, Lorincz A and Somogyi P 2000 Proximally targeted GABAergic synapses and gap junctions synchronize cortical interneurons *Nat. Neurosci.* **3** 366–71

Tang A, Bartels A and Sejnowski T 1997 Effects of cholinergic modulation on responses of neocortical neurons to fluctuating input *Cereb. Cortex* **7** 502–9

Tiesinga P, José J and Sejnowski T 2000 Comparison of current-driven and conductance-driven neocortical model neurons with Hodgkin–Huxley voltage-gated channels *Phys. Rev.* E **62** 8413–19

Tiesinga P and José J 2000 Robust gamma oscillations in networks of inhibitory hippocampal interneurons *Network* **11** 1–23

Tiesinga P 2001 Information transmission and recovery in neural communications channels revisited *Phys. Rev.* E **64** 012901

Tiesinga P, Fellous J-M, José J and Sejnowski T 2001a Computational model of carbachol-induced delta, theta and gamma oscillations in the hippocampus *Hippocampus* **11** 251–74

Tiesinga P, Fellous J-M, José J and Sejnowski T 2001b Optimal information transfer in synchronized neocortical neurons *Neurocomputing* **38–40** 397–402

Tiesinga P and Sejnowski T 2001 Precision of pulse-coupled networks of integrate-and-fire neurons *Network* **12** 215–33

Traub R, Whittington M, Colling S, Buzsaki G and Jeffreys J 1996a Analysis of gamma rhythms in the rat hippocampus *in vitro* and *in vivo J. Physiol.* **493** 471–84

Traub R, Whittington M, Colling S, Buzsaki G and Jeffreys J 1996b A mechanism for generation of long-range synchronous fast oscillations in the cortex *Nature* **383** 621–4

Wang X and Buzsáki G 1996 Gamma oscillation by synaptic inhibition in a hippocampal interneuronal network model *J. Neurosci.* **16** 6402–13

Warland D, Reinagel P and Meister M 1997 Decoding visual information from a population of retinal ganglion cells *J. Neurophysiol.* **78** 2336–50

Warzecha A and Egelhaaf M 1999 Variability in spike trains during constant and dynamic stimulation *Science* **283** 1927–30

Warzecha A, Kretzberg J and Egelhaaf M 1998 Temporal precision of the encoding of motion information by visual interneuron *Curr. Biol.* **8** 359–68

Wehr M and Laurent G 1996 Odor-encoding by temporal sequences of firing in neural assemblies *Nature* **384** 162–15

Wessel R, Gabbiani F and Koch C 1996 Coding of time-varying electric field amplitude modulations in a wave-type electric fish *J. Neurophysiol.* **75** 2280–93

White J, Chow C, Ritt J, Soto-Treviño C and Kopell N 1998 Synchronization and oscillatory dynamics in heterogeneous, mutually inhibited neurons *J. Comput. Neurosci.* **5** 5–16

Whittington M, Traub R and Jeffreys J 1995 Synchronized oscillations in interneuron networks driven by metabotropic glutamate receptor activation *Nature* **373** 612–5

Wiener M and Richmond B 1999 Using response models to estimate channel capacity for neuronal classification of stationary visual stimuli using temporal coding *J. Neurophysiol.* **81** 2861–75

Wiesenfeld K and Moss F 1995 Stochastic resonance and the benefits of noise: from ice ages to crayfish and SQUIDs *Nature* **373** 33–6